

Transdermal Photothermal-Pharmacotherapy to Remodel Adipose Tissue for Obesity and Metabolic Disorders

Ping Zan,[‡] Aung Than,[‡] Weiqing Zhang, Helen Xinyi Cai, Wenting Zhao, and Peng Chen*



Cite This: <https://doi.org/10.1021/acsnano.1c06410>



Read Online

ACCESS |



Metrics & More



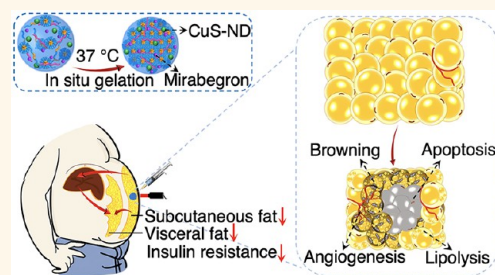
Article Recommendations



Supporting Information

ABSTRACT: Despite the increasing prevalence of obesity, the current medications, which act indirectly on the central nervous system to suppress appetite or on the gastrointestinal tract to inhibit fat absorption, suffer from poor effectiveness and side effects. Here, we developed a transdermal mild photothermal therapy directly acting on the root of evil (subcutaneous white adipose depot) to induce its ameliorating remodeling (browning, lipolysis, and apoptosis), based on the injectable thermoresponsive hydrogel encapsulated with copper sulfide nanodots. Further, combining pharmaceutical therapy with codelivery of mirabegron leads to a strong therapeutic synergy. This method not only ensures high effectiveness and low side effects due to localized and targeted application but also remotely creates significant improvements in systemic metabolism. Specifically, as compared to the untreated group, it totally inhibits obesity development in high-fat-diet fed mice (15% less in body weight) with decreased masses of both subcutaneous (40%) and visceral fats (54%), reduced serum levels of cholesterol (54%)/triglyceride (18%)/insulin (74%)/glucose (45%), and improved insulin sensitivity (65% less in insulin resistance index). This self-administrable method is amenable for long-term home-based treatment. Finally, multiple interconnected signaling pathways are revealed, providing mechanistic insights to develop effective strategies to combat obesity and associated metabolic disorders.

KEYWORDS: CuS nanodots, photothermal therapy, transdermal therapy, browning, obesity, metabolic disorders



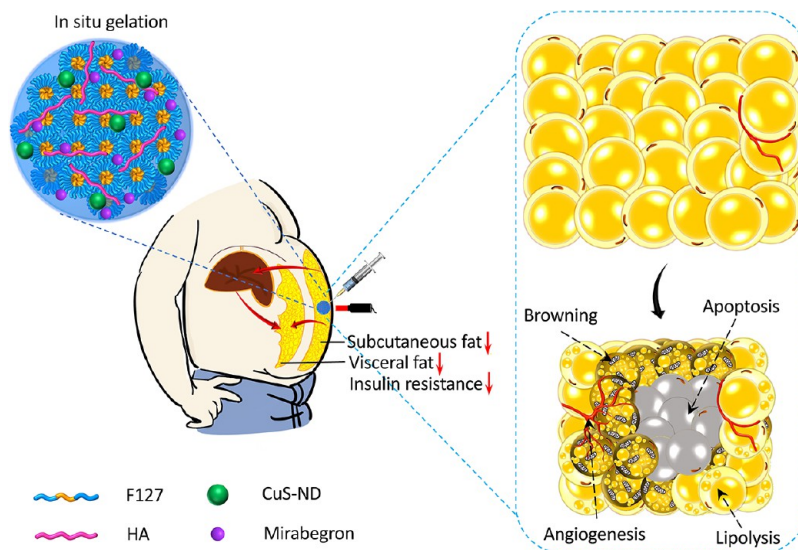
INTRODUCTION

White adipose tissue (WAT) not only stores energy in the form of triglycerides but also plays a pivotal role in body metabolism by secreting a family of metabolic factors called adipokines.¹ Excess accumulation of WAT or obesity, however, leads to other systemic metabolic disorders and subsequent development of devastating diseases, such as type 2 diabetes, cardiovascular diseases, stroke, and some cancers.^{2,3} This is largely imputable to over release of free fatty acids (FFA) and inflammatory cytokines as well as altered adipokine secretion from obese WAT.^{4,5} Despite its increasing prevalence, current interventions to combat obesity suffer from poor effectiveness and side effects.^{6–9} In contrast to WAT, brown adipose tissue (BAT) burns energy using glucose and FFA as the fuel, thereby mitigating the deleterious consequences of obesity.¹⁰ But BAT is scarce in adults. Intriguingly, brown-like beige adipocytes are inducible in WAT by certain activators through a browning process.^{11–14} As WAT is a dynamic, modifiable, and metabolically active tissue,¹⁵ stimulating its ameliorating remodeling is an effective strategy to combat obesity and associated metabolic disorders.

Transient receptor potential vanilloid 1 (TRPV1) ion channel, which is abundantly expressed in various cells including adipocytes, has recently received considerable attention for its role in energy homeostasis.^{16,17} Studies have shown that TRPV1 activation remodels WAT by promoting browning and lipolysis.^{18–20} As TRPV1 can be opened by capsaicin (the active ingredient of hot chili peppers), chronic dietary intake of capsaicin is found to reduce weight gain, adiposity, and blood level of triglycerides in animals and humans.^{21,22} However, capsaicin and its analogues cause irritation, pain, and a burning sensation to the skin and gastrointestinal track, as well as some adverse effects including diarrhea, nausea, and bronchitis.²³ Alternatively, TRPV1 can be activated by heat (>42 °C).^{24,25} Photothermal therapy (PTT), which converts high energy light

Received: July 28, 2021

Accepted: December 28, 2021

Scheme 1. Illustration of Transdermal Photothermal-Pharmacotherapy^{4†}

⁴HA: hyaluronic acid.

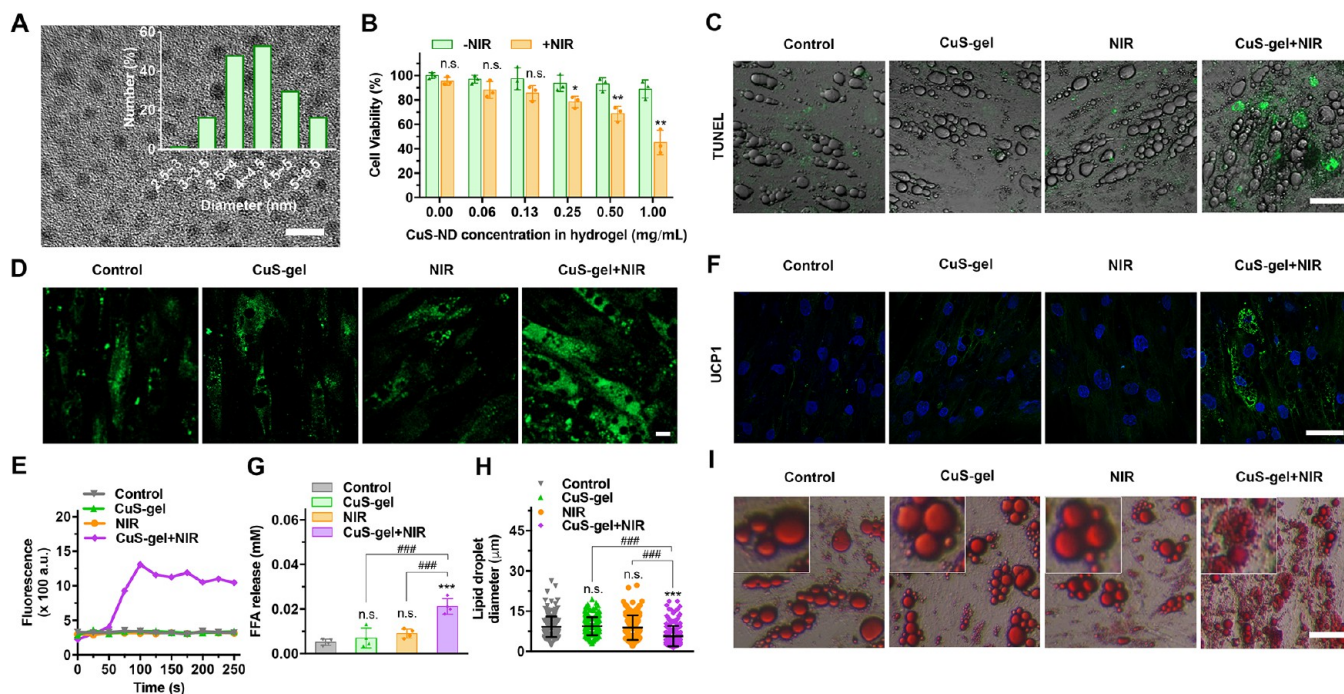


Figure 1. Characterization and mPTT effects of CuS-gel. mPTT was performed with NIR irradiation (1064 nm, 0.4 W/cm², 5 min) on CuS-gel (F127/HA hydrogel containing 0.5 mg/mL CuS-NDs or otherwise indicated) using human subcutaneous white adipocytes. (A) TEM image of CuS-NDs. Scale bar = 10 nm. Inset shows the size distribution ($n = 100$). (B) Viability of human subcutaneous adipocytes after incubation with CuS-gel containing different concentrations of CuS-NDs for 1d without (–) or with (+) NIR irradiation. Data represents mean \pm s.d. ($n = 3$). Two-tailed Student's *t* test (with versus without NIR): n.s. = not significant; * $P < 0.05$, ** $P < 0.01$. (C) Apoptosis indicated by TUNEL staining (green fluorescence). Scale bar = 50 μ m. (D) Fluorescence images and (E) quantified curves showing the change of intracellular calcium concentration. Scale bar = 10 μ m. (F) UCP1-labeled (green) immunofluorescence images with nuclei being stained blue. Scale bar = 50 μ m. (G) Release of free fatty acid (FFA) from adipocytes. Data represents mean \pm s.d. ($n = 4$). One-way ANOVA: n.s. = not significant; *** $P < 0.001$ versus control; ### $P < 0.001$ between indicated groups. (H) Diameters of intracellular lipid droplets (200 data points with mean and s.d. indicated). One-way ANOVA: n.s. = not significant; *** $P < 0.001$ versus control; ### $P < 0.001$ between indicated groups. (I) Oil Red O staining of intracellular lipid droplets. Scale bar = 50 μ m.

into intensive heat, has been widely utilized to ablate diseased tissues.^{26,27} We conceive that mild PTT (mPTT) transdermally delivered using tissue-penetrating second-window near-infrared light (NIR-II) and highly efficient PTT agents could stimulate TRPV1 signaling pathways, and combined with codelivery of

pharmaceuticals, beneficial remodeling of subcutaneous WAT (sWAT) depots would be synergistically induced (Scheme 1). The largest depot of WAT (belly fat in human, inguinal fat in mice), which is also readily accessible for transdermal therapy, would be the ideal site of treatment.

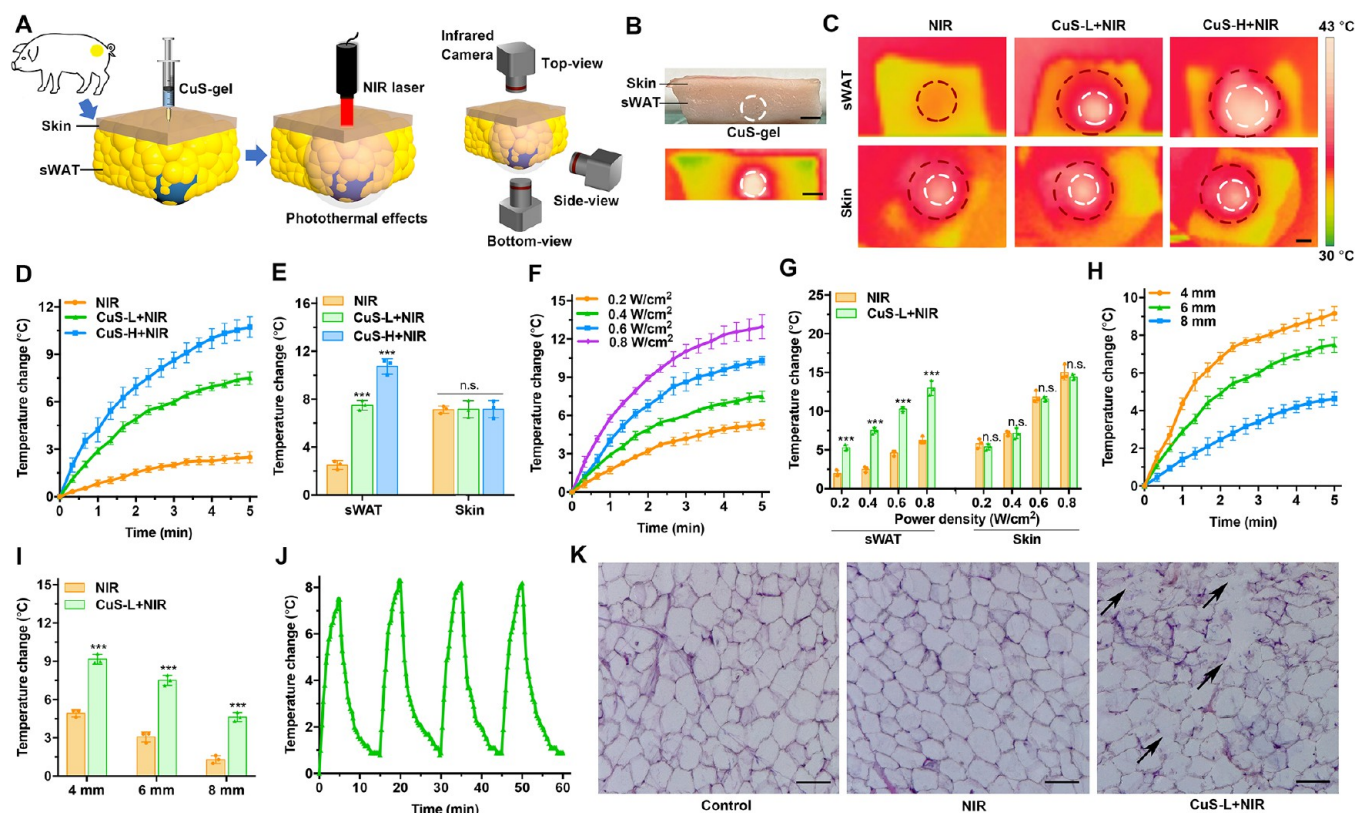


Figure 2. *Ex vivo* mPTT on porcine sWAT. CuS-L and CuS-H represents the hydrogels with low (0.5 mg/mL) and high (1 mg/mL) CuS-ND dosage. NIR refers to 5 min NIR irradiation with a power density of 0.4 W/cm² (unless otherwise indicated). All of the experiments were performed at 37 °C in an oven. All error bars represent standard deviation from three independent measurements. (A) Schematic illustration of the experiments. Porcine tissue (skin and sWAT) was cut with a thickness of 6 mm, and 100 μ L of CuS-gel was then injected into the bottom edge region for easy side-view and bottom-view thermal imaging. For experiments in (H) and (I), porcine tissues of 4 or 8 mm thick were also tested. (B) Bright field and infrared thermal images of skin and sWAT from side view under NIR irradiation. Scale bar = 3 mm. (C) Thermal images of sWAT (bottom-view) and skin surface (top-view) after NIR irradiation. Scale bar = 3 mm. (D) Real-time temperature changes of sWAT and (E) final temperature increase of sWAT and skin. One-way ANOVA: n.s. = not significant; *** P < 0.001 versus NIR group. (F) Real-time temperature changes of sWAT, and (G) final temperature increases of sWAT and skin after NIR irradiation at different power densities. Two-tailed Student's t test (CuS-L+NIR versus NIR group): n.s. = not significant; *** P < 0.001. (H) Real-time temperature changes, and (I) final temperature increases of sWAT at different depths. Two-tailed Student's t test (CuS-L+NIR versus NIR group): n.s. = not significant; *** P < 0.001. (J) Photothermal stability of CuS-L in sWAT for four NIR irradiation cycles. (K) Hematoxylin and eosin (H&E) staining images of sWAT. Scale bar = 100 μ m. Black arrows indicate membrane disruption of adipocytes.

Here, transdermal delivery of PTT and pharmaceutical agents is realized using a thermoresponsive hydrogel which is injectable at room temperature and quickly undertakes sol–gel transition inside sWAT to retain the cargos for sustained therapeutic effects. Copper sulfide nanodots (CuS-NDs) which possess high NIR-II photothermal conversion efficiency and good biocompatibility were chosen as the PTT agent. Impressively, the subsequent photothermal-pharmacotherapy (mPTT-PCT) totally inhibits obesity development in high-fat-diet fed mice. It not only locally leads to sWAT remodeling and mass reduction at the application site but also exerts significant improvements on whole-body metabolism including mass reduction of remote visceral fat. This strategy is highly translatable and amenable for home-based treatment. Furthermore, multiple interconnected signaling pathways are revealed to explain the high effectiveness, synergic therapeutic effects, and systemic influences produced by localized mPTT-PCT, thus providing key mechanistic insights for developing effective strategies to combat obesity and other metabolic disorders.

RESULTS AND DISCUSSION

CuS-gel and *In Vitro* mPTT on Human Subcutaneous Adipocytes. To choose a suitable photothermal agent for a chronic disease like obesity, biocompatibility, biodegradability, efficient NIR-II absorption, high photothermal conversion efficiency, and low synthesis cost are important considerations. Copper sulfide nanoparticles have been used as PTT agents for cancer therapy because of the stable and highly efficient NIR absorption derived from the d–d energy band transition of Cu²⁺ ions.^{28,29} In addition, Cu²⁺ is an essential element for human health and present in various foods and drinking water. Interestingly, it can promote angiogenesis,²⁸ which is desirable for remodeling low vascular density in obese WAT. Here, uniformly sized and citrate-capped CuS-NDs with a mean diameter of \sim 4 nm (Figure 1A) were readily synthesized based on a simple ionic reaction between copper chloride and sodium sulfide (Figure S1) in the presence of trisodium citrate surfactant for hydrophilic surface capping (Figure S2). Note that nanoparticles <6 nm can be easily cleared through the renal system.³⁰ CuS-ND exhibits strong absorption in the NIR-II region, which guarantees deep tissue penetration (Figure S3A).

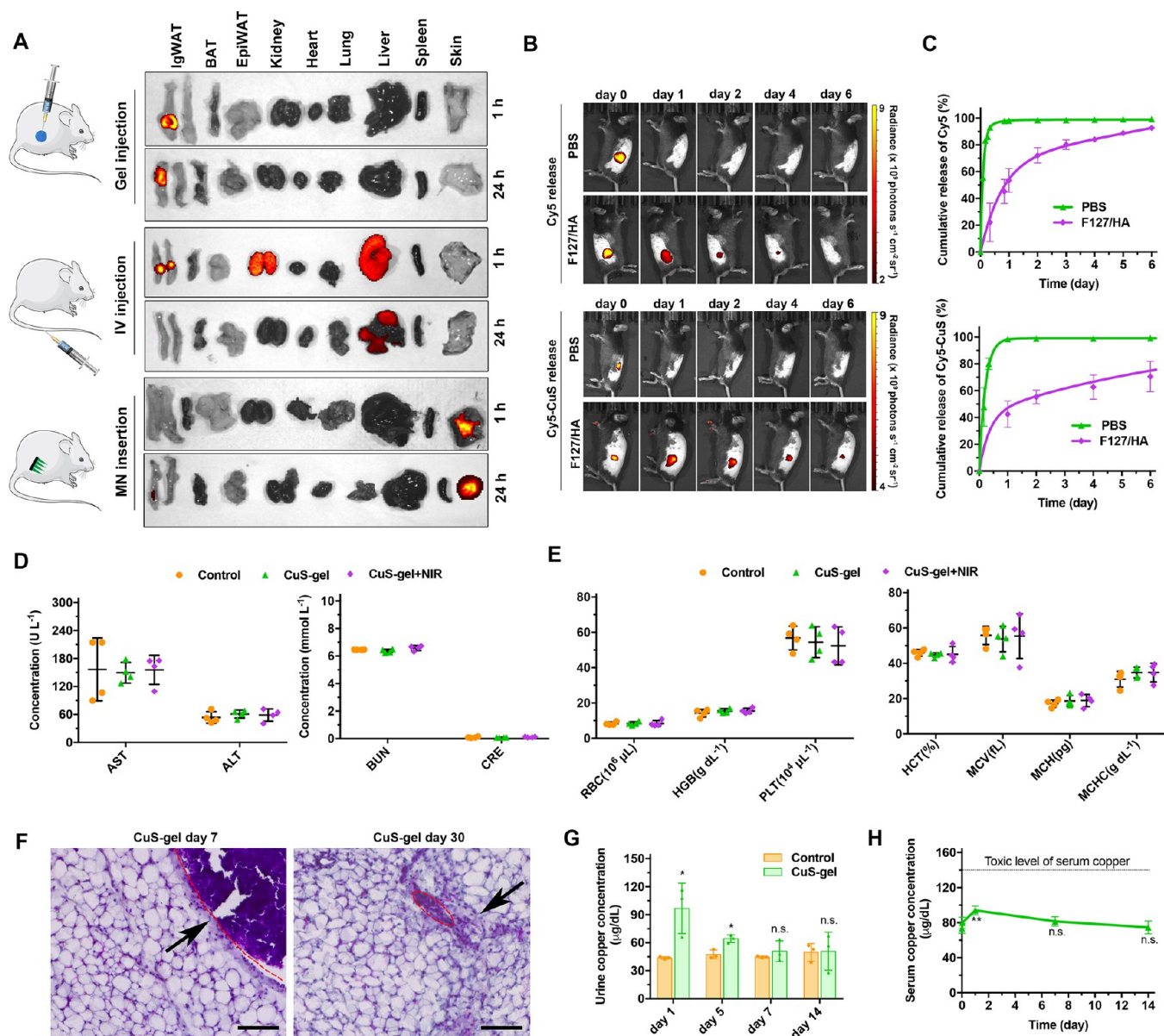


Figure 3. *In vivo* biodistribution, biocompatibility, and biodegradation of CuS-gel. (A) *In vivo* biodistribution of Cy5-CuS in major organs and fat tissues (inguinal WAT (IgWAT), epididymal WAT (EpiWAT), brown adipose tissue (BAT)) of mice, 1 or 24 h after subcutaneous injection of CuS-gel (50 μ L loaded with 25 μ g Cy5-CuS), or IV injection of 25 μ g Cy5-CuS or application of dissolving microneedle (MN) patch encapsulated with 25 μ g of Cy5-CuS onto one side of the inguinal region. (B) *In vivo* fluorescence images and (C) quantitative release profiles of Cy5 and Cy5-CuS after subcutaneous injection of Cy5/Cy5-CuS incorporated in F127/HA gel or dispersed in PBS solution (pH 7.4). Data represents mean \pm s.d. ($n = 4$ mice per group). (D) Serum levels of liver function indicators (aspartate transaminase (AST), alanine transaminase (ALT)), kidney function indicators (blood urea nitrogen (BUN), creatinine (CRE)). (E) Blood analysis: red blood cell (RBC), hemoglobin (HGB), platelet (PLT), hematocrit (HCT); mean corpuscular volume (MCV), mean corpuscular hemoglobin (MCH), mean corpuscular hemoglobin concentration (MCHC), in control mice or mice subcutaneously injected with CuS-gel into two sides of IgWAT once a week or mice with CuS-gel injection followed by NIR irradiation (1064 nm, 0.4 W/cm², 5 min) for 3 consecutive days. The treatment was repeated for 2 weeks. Data represents mean \pm s.d. ($n = 4$ mice per group). One-way ANOVA: n.s. = not significant versus control group. (F) Histological images of IgWAT from mice subcutaneously injected with CuS-gel at day 7 and day 30. Areas highlighted by red lines indicate CuS-gel, and black arrows indicate mononuclear cells. Scale bar = 100 μ m. (G,H) Serum and urinary copper concentration in control mice and mice subcutaneously injected with CuS-gel. Data represents mean \pm s.d. ($n = 3$ mice per group). Two-tailed Student's *t* test (CuS-gel treated versus control): n.s. = not significant; **P* < 0.05, ***P* < 0.01. The mouse drawing is reproduced with permission under a Creative Commons Attribution 3.0 Unported License from Servier Medical Art; <https://smart.servier.com>. Copyright 2020 Servier Laboratories.

Hence, compared to other PTT agents, CuS-ND is ideal for transdermal PTT for obesity.

Pluronic F127, an FDA-approved nonionic surfactant, was chosen as the delivery vehicle because it is fluidic at a low temperature to allow syringeability and undergoes a quick sol-gel transition at body temperature to avoid burst discharge of

therapeutics. This is ascribed to the promoted formation of F127 micelles *via* self-assembly by the hydrophobic interaction between their poly(propylene oxide) (PPO) blocks at elevated temperatures and subsequent rearrangement into highly ordered cubic or hexagonal structures (Figure S4). The sustainability was further enhanced by adding high-molecular-

weight (~ 1000 kDa) hyaluronic acid (HA) which cross-links F127 micelles through hydrogen bonding and hydrophobic interaction between its acetyl groups and methyl groups on F127 (Figure S5).³¹ With only 1% HA, the time constant for *in vitro* release of Cy5 dye molecules (as drug model) from gelled F127 (25%) increases from 1.4 to 3.9 days (Figure S3B). Moreover, HA helps to rectify low-grade inflammation in obese WAT. Similar to blank F127/HA hydrogel, CuS-ND incorporated hydrogel (CuS-gel) is fluidic at 4 °C and even at room temperature for ~ 10 min and transforms into an elastic solid at 37 °C (Figure S3C). Under NIR-II (1064 nm) laser irradiation, the temperature of CuS-gel increased in a dose, time, and laser-power dependent manner with high photostability, e.g., ΔT of 12.6 °C after 5 min irradiation (0.4 W/cm^2) with 0.5 mg/mL CuS-ND (Figure S6). Altogether, CuS-gel simultaneously achieves injectability, sustainability, good photothermal effect, and the ability to carry other therapeutics.

CuS-gel exhibited negligible cytotoxicity to human subcutaneous adipocytes, whereas cell viability significantly decreased after laser irradiation when the CuS-ND concentration >0.25 mg/mL (Figure 1B). Consistently, terminal deoxynucleotidyl transferase dUTP nick end labeling (TUNEL) in nucleus indicated that some adipocytes underwent apoptosis after mPTT (Figure 1C). Activation of TRPV1 channels was evidenced by the sharp increase of intracellular calcium concentration upon mPTT (Figure 1D,E). The high expression of uncoupling protein 1 (UCP1), a brown-adipocyte specific mitochondrial protein responsible for thermogenic respiration, appeared after mPTT, suggesting that white adipocytes transformed into brown-like adipocytes through TRPV1-mediated pathways (Figures 1F and S7). Furthermore, triggered lipolysis was confirmed by an increased release of FFA (Figure 1G) and a decreased size of intracellular lipid droplets (Figure 1H,I). The similar performance of CuS-NDs without gel encapsulation suggests that the observed biological responses are attributable to the photothermal property of CuS-NDs (Figure S8). Taken together, mPTT is able to induce apoptosis, browning, and lipolysis of human white adipocytes.

Ex vivo mPTT on Porcine sWAT. Closely resembling human skin, porcine skin is ~ 2 mm thick and has attached sWAT. Therefore, porcine sWAT was used as the *ex vivo* model to prove the practical feasibility of applying transdermal mPTT on human abdominal sWAT (Figure 2A). Specifically, a single-injection of CuS-gel (100 μL) was administrated into porcine sWAT using a thin insulin needle (32-gauge) whose insertion is considered virtually painless. Under mild NIR-II irradiation (0.4 W/cm^2 , 5 min) above the skin, the temperature of CuS-gel (0.5 mg/mL CuS-NDs) embedded at ~ 6 mm deep inside sWAT increased from 32.5 to 40 °C ($\Delta T = 7.5$ °C) and it heated the surrounding tissue to 36 °C (Figure 2B). Doubling the CuS-ND dosage led to a ΔT of 10.7 °C, while without a CuS-gel the temperature increase was only 2.5 °C (Figure 2C–E). With or without CuS-gel, the skin surface temperature rose similarly by 7 °C. These results demonstrate that, under *in vivo* conditions (skin and sWAT temperature of ~ 34 and 37 °C), such mPTT is sufficient to activate the TRPV1 channel (>42 °C) in sWAT yet without heating the skin above 44 °C, which is the threshold to cause pain (exposure for seconds) and burning (exposure for hours). Lowering the laser power to 0.2 W/cm^2 may still be able to activate TRPV1 ($\Delta T = 5.3$ °C), but likely with compromised therapeutic efficacy. The balance between efficacy and biosafety can be tailored by the laser power and CuS-ND concentration (Figure 2D,F). Although NIR alone with a higher power (0.8

W/cm^2) increased the sWAT temperature by 6.2 °C, it warmed the skin by 15 °C, which would cause skin damage (Figure 2G). In the following experiments, unless otherwise stated, CuS-gel with 0.5 mg/mL CuS-NDs and 5 min irradiation of 0.4 W/cm^2 NIR were used for mPTT. Using these parameters, effective mPTT-induced sWAT remodeling can be realized within 6 mm depth (Figure 2H,I) with high stability under repetitive stimulation (Figure 2J). As revealed by H&E staining (Figure 2K), mPTT (but not NIR alone) caused disruption of the cell membrane, thereby allowing release of intracellular lipids (lipolysis).

In Vivo Biosafety and Biodistribution in Mice. In order to track CuS-NDs in mice, CuS-NDs were conjugated with fluorescent dye Cy5 molecules *via* covalent bonding between the COOH groups of citrate molecules capped on CuS-NDs and amide handles on the fluorophores. Biodistribution of Cy5-conjugated CuS-ND (Cy5-CuS) resulting from subcutaneous injection of Cy5-CuS-loaded F127/HA into mouse inguinal WAT (IgWAT, equivalent to large sWAT depot in human) was imaged and compared with systemic delivery using intravenous (IV) injection and transdermal delivery using a polymeric microneedle (MN) patch (Figures 3A and S9). To enhance the WAT-targeting ability of IV injection, Cy5-CuS was further functionalized with adipose-homing peptide (CKGGRKDC), which specifically binds to prohibitin expressed abundantly on adipocytes and endothelial cells of adipose vasculature.³² But $\sim 70\%$ of Cy5-CuS still quickly accumulated in liver and kidney 1 h after IV injection, while only $\sim 20\%$ reached IgWAT. After 24 h, there was almost no Cy5-CuS remaining in IgWAT. Clearly, even using the currently most appreciated targeting moiety, conventional systemic administration cannot efficiently deliver therapeutics into adipose tissue, which lacks highly specific biomarkers. It is worth mentioning that, using intraperitoneal (IP) injection, dextran nanocarriers promote drug delivery into visceral WAT in mice.³³ But, for humans, IP injection can only be administered by trained medical professionals and is associated with pain and risk of internal injury. Drug delivery based on dissolvable polymeric MNs is advantageous in terms of minimal invasiveness and high bioavailability.^{34,35} Self-administrable MN skin patches have been employed for delivery of antiobesity molecules into dermis, which then reach sWAT by diffusion.^{36–38} Delivered by MNs made of dissolving hyaluronic acid, only a small fraction of Cy5-CuS gradually diffuses into IgWAT due to its high molecular weight (~ 105 kDa), while $\sim 90\%$ remained in the skin even after 1 day (Figures 3A and S9). In this case, mPTT would cause skin burning and ineffective therapy in sWAT. In contrast, nearly all Cy5-CuS was retained in IgWAT 1 h after injection of CuS-gel using an insulin needle, owing to fast *in situ* gelation of F127/HA. After 24 h, 58% still remained in IgWAT, and its accumulation in kidney and liver (but not heart, lung, and spleen) suggested that after entering circulation CuS-NDs would largely be cleared by renal and hepatobiliary excretion. *In vivo* release of the Cy5 molecule (as drug model) and Cy5-CuS (as PTT agent) from F127/HA hydrogel lasted several days, in sharp contrast to the burst release (<1 h) when PBS was used as the delivery vehicle (Figure 3B,C).

Biocompatibility of CuS-gel-based mPTT was attested by major organ histology and blood analyses. Specifically, there was no detectable hepatic, renal, splenic, pulmonary, and cardiac necrosis, congestion, or hemorrhage (Figure S10), and there were no significant differences between control mice and treated mice in terms of blood biomarkers for hepatic (aspartate transaminase (AST) and alanine transaminase (ALT)), renal

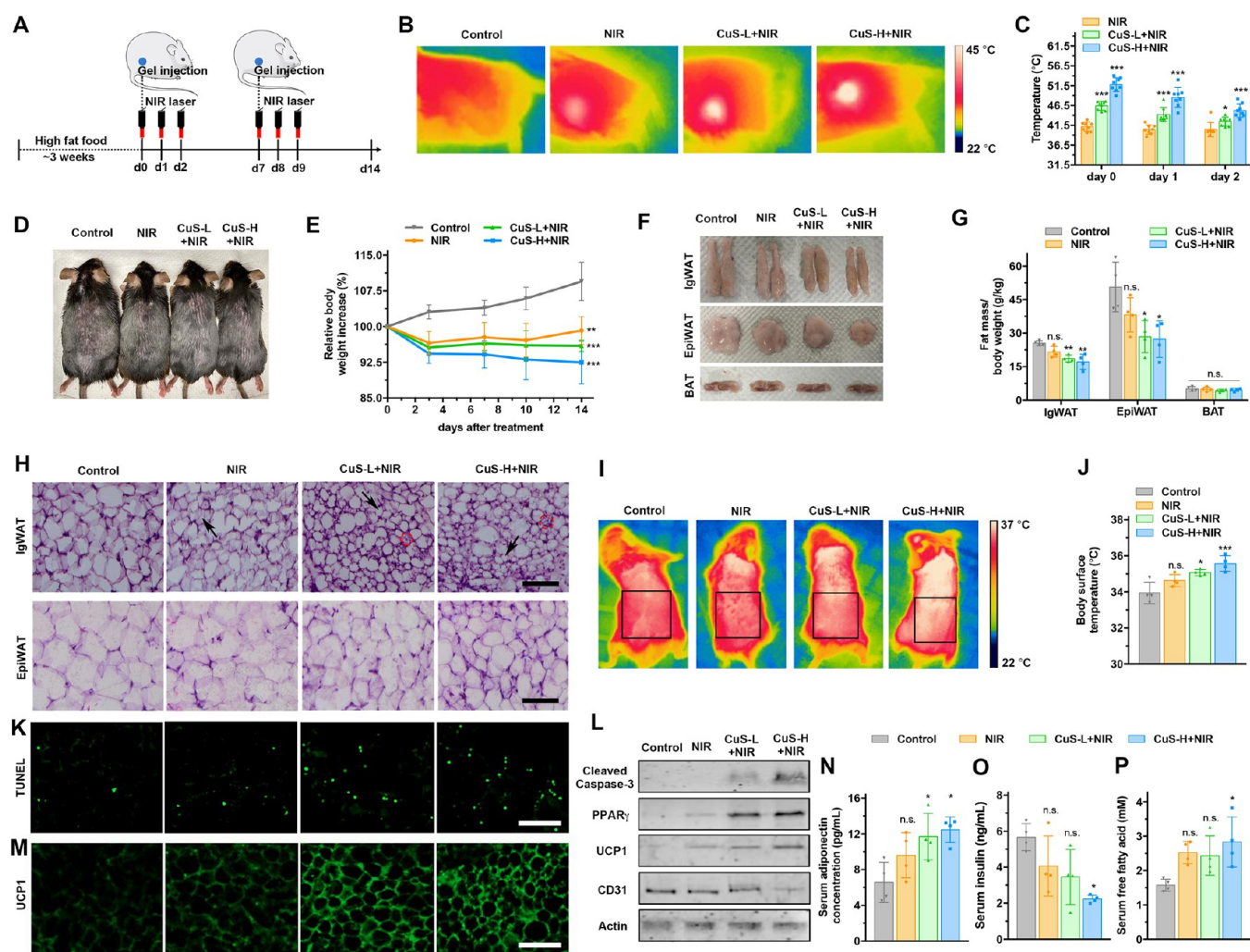


Figure 4. *In vivo* mPTT efficacy on obese mice. CuS-gel was injected subcutaneously at both sides of the inguinal regions once a week, followed by NIR laser irradiation (1064 nm, 0.4 W/cm², 5 min) for 3 consecutive days. The treatment was repeated in the second week. CuS-L and CuS-H represent the hydrogels with low (in gel: 0.5 mg/mL; in mouse: 1.5 mg/kg) and high (in gel: 1 mg/mL; in mouse: 3 mg/kg) CuS-ND dosage. (A) Protocol illustration. (B) Thermal images and (C) skin temperature after NIR irradiation. Data represents mean \pm s.d. ($n = 8$). One-way ANOVA: * $P < 0.05$, *** $P < 0.001$ versus NIR group. (D) Photographs of differently treated mice at day 14. (E) Relative body weight changes over the course of treatment. (F) Photographs and (G) relative fat mass of IgWAT, EpiWAT, and interscapular BAT at day 14. Data represents mean \pm s.d. ($n = 4$ mice per group). One-way ANOVA: n.s. = not significant; * $P < 0.05$, ** $P < 0.01$ versus control. (H) H&E staining images of IgWAT and EpiWAT. Black arrow indicates a representative adipocyte with smaller size due to lipolysis; circle indicates a representative brown-like adipocyte with multilocular morphology. Scale bar = 100 μ m. (I) Thermal images and (J) average body surface temperature (from the indicated inguinal area) of differently treated mice at day 14. Data represents mean \pm s.d. ($n = 4$ mice per group). One-way ANOVA: n.s. = not significant; * $P < 0.05$, *** $P < 0.001$ versus control. (K) TUNEL staining (green fluorescence) of IgWATs after different treatments. Scale bar = 100 μ m. (L) Immunoblots of cleaved caspase-3, PPAR γ , UCP1, CD31, and actin in IgWAT. (M) UCP1-labeled (green) immunofluorescence images of IgWATs after different treatments. Scale bar = 100 μ m. (N–P) Serum levels of adiponectin, insulin, and free fatty acids (FFA). Data represents mean \pm s.d. ($n = 4$ mice per group). One-way ANOVA: n.s. = not significant; * $P < 0.05$ versus control. The mouse drawing is reproduced with permission under a Creative Commons Attribution 3.0 Unported License from Servier Medical Art; <https://smart.servier.com>. Copyright 2020 Servier Laboratories.

(blood urea nitrogen (BUN) and creatinine (CRE)) and hematologic (red blood cell (RBC), platelet (PLT), and hemoglobin (HGB)) functions (Figure 3D,E). Furthermore, signs of pain as evaluated by Grimace scoring, damage on skin surface, and abnormalities in skin histology were absent (Figure S11).

It has been shown that CuS nanoparticles are biodegradable.³⁹ Biodegradability of CuS-gel was investigated. As shown in Figure 3F, CuS-gel embedded in IgWAT was surrounded by a thin layer of mononuclear cells and vanished after a month without causing alterations to IgWAT. Cu²⁺ concentration in

urine showed a significant increase at day 1 and restored after day 5 (Figure 3G), confirming that CuS-NDs were mainly metabolized by renal excretion. Only at day 1 was the serum level of Cu²⁺ increased by 28% to 94.01 μ g/dL, which is still much lower than the toxic threshold of 140 μ g/dL (Figure 3H).

Localized and Systemic Antiobesity Effects of mPTT.

The antiobesity effects of mPTT were further investigated on an obese mouse model established by feeding the mice with a high fat diet (HFD) (Figure 4A). After 3 weeks, hyperglycemia and insulin resistance were observed in HFD-fed mice (but not in normal chow fed mice), suggesting the development of obesity

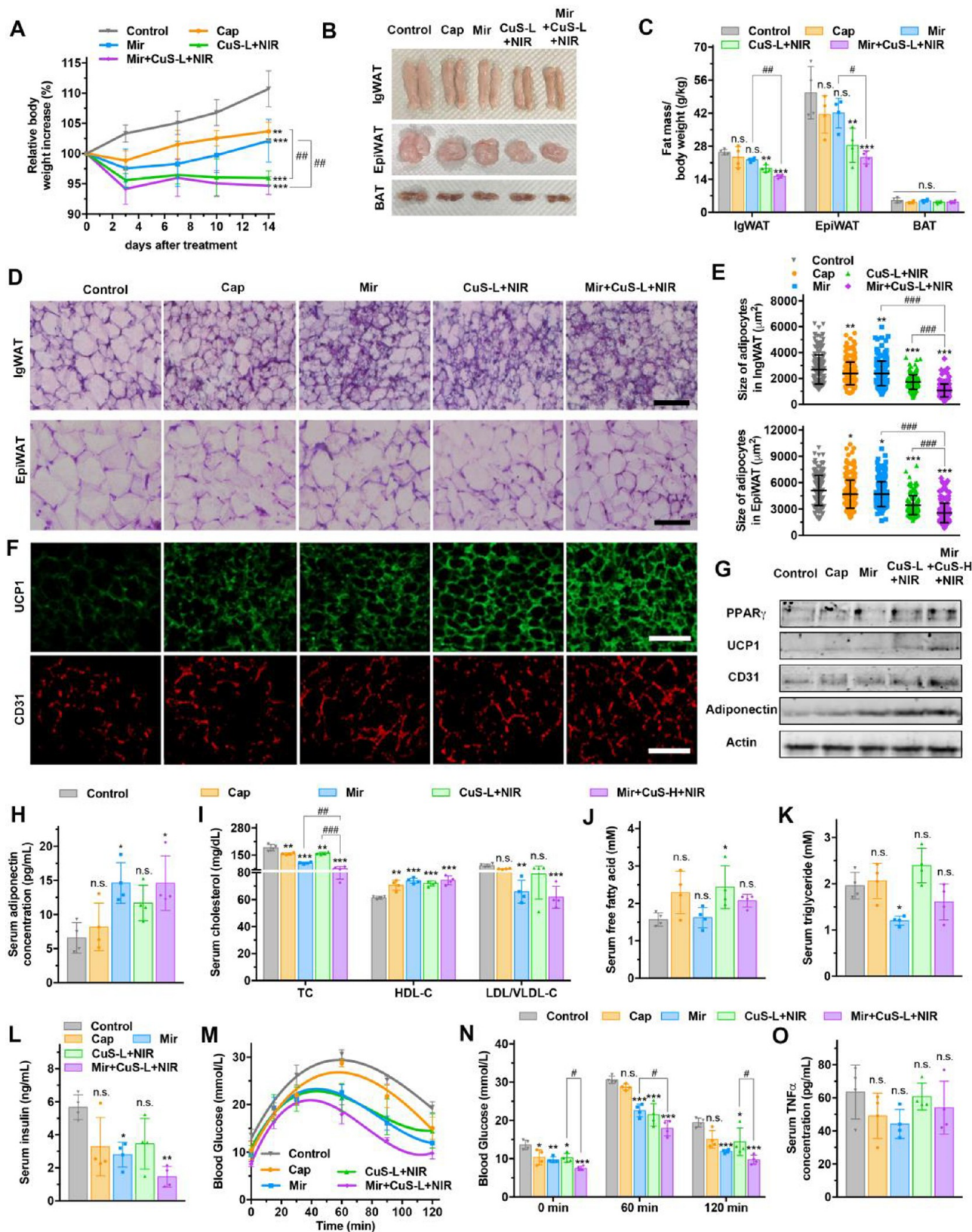


Figure 5. mPTT-PCT suppresses obesity and associated metabolic disorders. Experiments follow the same protocol as in Figure 4. In some, the hydrogel contains capsaicin (Cap, 3 mg/kg) or mirabegron (Mir, 0.75 mg/kg). (A) Relative body weight changes of mice over the course of treatment. (B) Photographs and (C) relative fat masses of IgWAT, EpiWAT, and interscapular BAT at day 14. In (A) and (C), data represents mean \pm s.d. ($n = 4$ mice per group). One-way ANOVA: n.s. = not significant; ** $P < 0.01$, *** $P < 0.001$ versus control; # $P < 0.05$, ## $P < 0.01$ between indicated groups. (D) H&E staining images of IgWAT and EpiWAT. Scale bar = 100 μ m. (E) Adipocyte sizes (200 data points with mean and s.d. indicated). One-way ANOVA: n.s. = not significant; * $P < 0.05$, ** $P < 0.01$, *** $P < 0.001$ versus control; #### $P < 0.001$ between indicated groups. (F) UCP1-labeled (green) and CD31-labeled (red) immunofluorescence images of IgWATs after different treatments. Scale

Figure 5. continued

bar = 100 μm . (G) Immunoblots of PPAR γ , UCPI, CD31, adiponectin, and actin in IgWATs. (H–L) Serum levels of adiponectin, TC, HDL-C, LDL/VLDL-C, FFA, triglyceride, and insulin. Data represents mean \pm s.d. ($n = 4$ mice per group). One-way ANOVA: n.s. = not significant; * $P < 0.05$, ** $P < 0.01$, *** $P < 0.001$ versus control; # $P < 0.01$, ### $P < 0.001$ between indicated groups. (M) Change of blood glucose level after glucose solution (1 g/kg in PBS) was intraperitoneally injected at $t = 0$ min. (N) Blood glucose levels at various time points. Data represents mean \pm s.d. ($n = 4$ mice per group). One-way ANOVA: n.s. = not significant; * $P < 0.05$, ** $P < 0.01$, *** $P < 0.001$ versus control; # $P < 0.05$ between indicated groups. (O) Serum level of TNF α . Data represents mean \pm s.d. ($n = 4$ mice per group). One-way ANOVA: n.s. = not significant.

associated metabolic syndromes (Figure S12). Subsequently, different treatments were performed with continuous HFD feeding. For mPTT, CuS-gel (CuS-ND dose in gel: 0.5 mg/mL; in mouse: 1.5 mg/kg) was injected into the inguinal region, and the skin temperature rose to ~ 45 $^{\circ}\text{C}$ after 5 min NIR irradiation (Figure 4B,C). As mouse skin thickness is only ~ 0.6 mm, the temperature in the underneath IgWAT is similar (Figure S13). With a higher CuS-ND dose (1 mg/mL), the skin temperature increased to >50 $^{\circ}\text{C}$, causing severe skin burning (Figure S14). A 5 min mPTT treatment was given for 3 consecutive days, followed by 4 days of rest to complete one course of treatment (1 week). The induced temperature rise slightly decreased over time due to gradual loss of CuS-NDs from the gel (Figure 3B).

Impressively, mPTT completely inhibited obesity development (Figures 4D,E and S15A). Specifically, without treatment, mouse body weight gained 9.5% over 2 weeks whereas mPTT with low-dose or high-dose CuS-gel caused a weight decrease of 4.1% or 7.6%. Noteworthy, NIR irradiation alone also caused 0.8% weight reduction, suggesting that some PTT effects are created due to thin thickness of mouse skin. But NIR alone is not sufficient to achieve mPTT for sWAT underneath porcine (Figure 2B,G) or human skin without causing skin burning. CuS-gel injection without NIR failed to show any antiobesity effect (Figure S16A). Note that food intake, urine volume, and feces weight were almost identical for all mouse groups (Figures S15B, S16B, and S17A,B). In addition, the stress level is similar for all groups, as indicated by the serum level of corticosterone, the main stress hormone in rodents (Figure S17C).

Subcutaneous IgWAT and visceral epididymal WAT (EpiWAT) significantly shrunk in both mPTT groups (27 and 33% less for IgWAT; 44 and 46% less for EpiWAT) (Figure 4F,G). Large reduction of visceral fat implies that localized subcutaneous treatment on IgWAT exerts systemic antiobesity effects. Furthermore, size reduction of adipocytes in both WATs was observed (Figures 4H and S15C,D), resulting from lipolysis. Notably, thermogenic multilocular brown-like adipocytes appeared in IgWAT after mPTT (Figure 4H), indicating browning of IgWAT. Browning was further confirmed by elevated body temperature at inguinal regions (Figure 4I and J). As revealed by TUNEL staining, apoptosis in IgWAT was also induced by mPTT (Figure 4K).

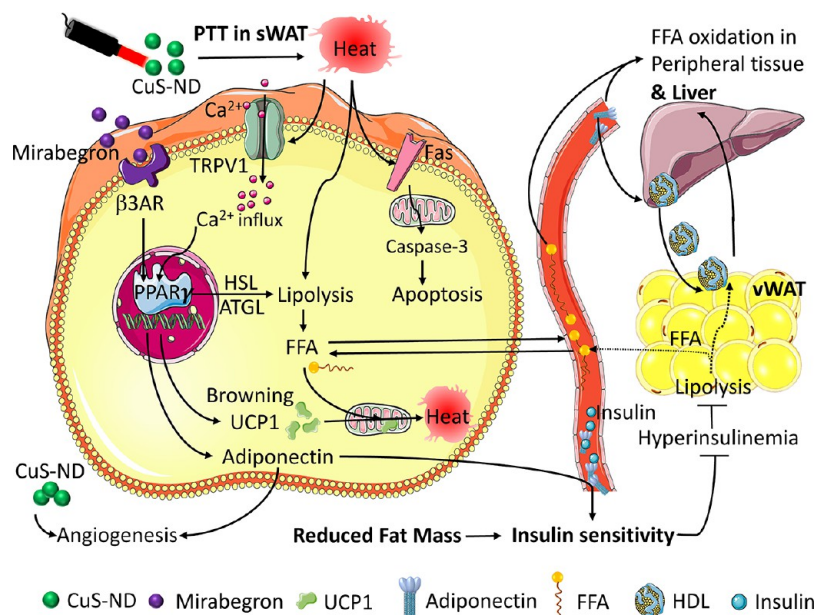
The antiobesity mechanism was further investigated at the molecular level. Caspase-3, a key effector to execute the apoptotic program, was activated (Figures 4L and S18), confirming triggered apoptosis in IgWAT. Peroxisome proliferator-activated receptor gamma (PPAR γ), a nuclear receptor playing the key role in browning, was also significantly augmented. This in turn promoted expression of thermogenic protein UCPI (Figures 4L,M, S18, and S19). Expression of endothelial cell marker CD31 was not altered, meaning that mPTT did not damage adipose vasculature. But doubling the CuS-ND dosage (3 mg/kg) to further enhance the slimming effect (Figure 4, panels D–G) undesirably led to a significant decrease of CD31 levels (Figures 4L and S18). Skin burning and

blood vessel damage caused by PTT with a high CuS-ND dose restricts its practical implementation. Thus, 1.5 mg/kg (0.5 mg/mL in gel) is preferred because of the optimal balance between antiobesity effectiveness and safety. Desirably, mPTT did not trigger inflammatory response as indicated by the unchanged TNF α level (Figure S20A).

Among various adipokines, WAT secretes adiponectin, which has anti-inflammatory and insulin-sensitizing properties.⁴⁰ Interestingly, mPTT stimulated adiponectin production (Figure 4N), likely due to activation of TRPV1-PPAR γ signaling (Figures 1D and 4L).⁴¹ After mPTT, the serum insulin level was desirably reduced owing to increased insulin sensitivity whereas FFA was undesirably elevated owing to triggered lipolysis (Figure 4O,P). Therefore, obesity-associated insulin resistance (insulin level \times FFA level) was not improved by mPTT (Figure S21). High serum levels of total cholesterol and triglycerides in obese mice were also not suppressed by mPTT (Figure S20B,C). Advantageously, the serum level of high-density lipoproteins (HDL) that remove lipids from peripheral tissues to liver was significantly increased, whereas low-density lipoprotein/very low-density lipoproteins (LDL/VLDL) that carry lipids to peripheral tissues were decreased (Figure S20B), likely because increased adiponectin secretion influenced their synthesis in liver.⁴²

Synergistic Effects of mPTT-PCT on Obesity and Metabolic Disorders. Capsaicin is a potent TRPV1 agonist known for its browning capability. Here, we observed that antiobesity efficacy of mPTT was significantly superior to that of capsaicin treatment based on the same hydrogel delivery and doubled dosage (3 mg/kg) than CuS-ND (Figures 5A and S22). This implies that mPTT is more potent and also stimulates antiobesity signaling pathways independent of TRPV1. Prolonged or repeated application of capsaicin leads to desensitization of TRPV1.²⁴ In comparison, mPTT controllably activates TRPV1 channels only 5 min per day. Nevertheless, mPTT did not effectively improve hyperlipidaemia and insulin resistance (Figures S20B,C and S21). We therefore conceived that combining mPTT and pharmacotherapy (mPTT-PCT) should create synergy to tackle systemic metabolic disorders.

Mirabegron, a β_3 adrenergic receptor ($\beta_3\text{AR}$) agonist approved by the US-FDA for overactive bladder syndrome, can improve glucose and lipid homeostasis and promote browning and lipolysis in obese humans and mice.^{43,44} We encapsulated both mirabegron and CuS-ND in the hydrogel for mPTT-PCT and compared it to treatments with mPTT, mirabegron, or capsaicin alone. Mice lost more weight by mPTT compared to PCT (mirabegron treatment) (Figures 5A and S22B) because of the multifaceted antiobesity effects of mPTT and desensitization of $\beta_3\text{AR}$ in the sustained presence of mirabegron.⁴⁵ As anticipated (Figure 5A–C), the mice after synergistic mPTT-PCT had the lowest body weight (15% lower than control) and smallest fat mass (40% less IgWAT and 54% less EpiWAT than control). Furthermore, mPTT-PCT was most potent in reducing adipocyte hypertrophy in both directly

Scheme 2. Illustration of the Localized and Systemic Anti-Obesity Mechanisms by Photothermal-Pharmacotherapy^a

^asWAT: subcutaneous white adipose tissue; vWAT: visceral white adipose tissue; FFA: free fatty acid; β 3AR: beta-3 adrenergic receptor; TRPV1: transient receptor potential vanilloid 1; PPAR γ : peroxisome proliferator-activated receptor gamma; UCP1: uncoupling protein 1; VEGF: vascular endothelial growth factor; HDL: high-density lipoprotein; HSL: hormone-sensitive lipase; ATGL: adipose triglyceride lipase. The drawings of cell structure, nucleus, membrane proteins, mitochondria, vessel, liver, lipoprotein and insulin are reproduced with permission under a Creative Commons Attribution 3.0 Unported License from Servier Medical Art; <https://smart.servier.com>. Copyright 2020 Servier Laboratories.

treated IgWAT and remote EpiWAT due to lipolysis of intracellular lipid droplets in both WATs and appearance of multilocular brown-like adipocytes in IgWAT (Figure 5D,E). mPTT-PCT treated mice also showed the highest inguinal surface temperature (Figure S23A,B), further confirming significant browning. Presumably, FFAs resulting from lipolysis are largely consumed by the nearby transformed brown-like adipocytes to produce heat.

All treatments enhanced PPAR γ and UCP1 expression in IgWAT, implying that browning is realized through the collaboration between the two signaling pathways (Figures 5F,G, S24, and S25). Consistently, mPTT-PCT gave the highest enhancement. Additionally, CD31 level was largely augmented in mPTT-PCT (but not PCT or mPTT alone), indicating that the two therapies synergistically promote microvascularization. In agreement with the previous reports,⁴¹ increase of PPAR γ also promoted secretion of adiponectin from IgWAT into circulation (Figures 5G,H and S25), which is beneficial to systemic metabolism.⁴⁰ Among the treatments, mPTT-PCT desirably led to the lowest total cholesterol, lowest LDL/VLDL, and highest HDL level in serum (Figure 5I). In contrast to mPTT alone, mPTT-PCT did not cause an increase of FFA in serum (Figure 5J) because conceivably the combined therapy enabled stronger browning effect and thus more consumption of FFA as the fuel by brown-like adipocytes. Pharmacotherapy by mirabegron reduced serum level of triglycerides (Figure 5K) presumably because of lipolysis by hormone-sensitive lipase (HSL) which was stimulated by PPAR γ signaling. But mPTT and mPTT-PCT did not significantly decrease serum triglyceride levels, likely because of the balance between the two distinct lipolysis processes, *i.e.*, triglyceride release due to direct thermal melting of lipid droplets and breakdown of triglyceride due to increased expression of lipases (HSL and ATGL) (Figure S26). Only mPTT-PCT treatment largely

suppressed hyperinsulinemia and insulin resistance associated with obesity (Figure 5L and S23C). mPTT-PCT most effectively lowered the fasting blood glucose level (diabetes indicator) to 7.5 mM (13.6 mM for control mice) and facilitated glucose clearance in blood after glucose injection (Figure 5M,N). Notably, the serum level of TNF α remained constant (Figure 5O), indicating that mPTT-PCT did not elicit inflammatory response.

Multiple Interconnected Signaling Pathways Evoked by mPTT-PCT. On the basis of our experimental observations, multifaceted antiobesity effects induced both locally and systemically by localized transdermal mPTT-PCT are attributed to activation of multiple interconnected signaling pathways (Scheme 2). First, heat generated by mPTT at the laser focal point triggers rapid programmed death of some adipocytes through the mitochondrial pathway as indicated by increased activation of caspase-3, possibly mediated by the Fas receptor. Simultaneously, heat stimulates lipolysis by converting the liquid-crystalline state of lipid droplets into a less ordered liquid state that enhances accessibility by lipases and carrier proteins.⁴⁶ Second, the spreading heat opens TRPV1 channels on the nearby adipocytes. The elicited calcium influx activates PPAR γ receptors in the nucleus through a signaling cascade, which in turn stimulates expression of thermogenic protein UCP1 in mitochondria and promotes expression of lipases (HSL and ATGL) for lipolysis of triglyceride into FFA. Third, stimulation of β 3AR membrane receptors by mirabegron also activates PPAR γ to induce browning and lipolysis. Browning was proved by the increase of UCP1, multilocular morphology of adipocytes, and increased body surface temperature of mice. Lipolysis was evidenced by reduced cell size. Released FFAs from lipolysis are consumed by the transformed brown-like adipocytes to generate heat.

Intriguingly, PPAR γ also stimulates the secretion of adiponectin from sWAT into circulation. Both Cu²⁺ (Figure S16C,D) and adiponectin promote angiogenesis,^{47,48} which in turn contributes to browning through paracrine interactions between endothelial cells and adipocytes.⁴⁹ Furthermore, adiponectin promotes insulin sensitivity and FFA oxidation in peripheral tissues and liver, leading to enhanced glucose uptake and reduced hepatic gluconeogenesis.⁴⁰ Consequently, hyperglycaemia, hyperinsulinemia, and insulin resistance associated with obesity are largely repressed. Inhibition of lipolysis in visceral WAT (vWAT) by hyperinsulinemia is thus relieved. Additionally, adiponectin promotes hepatic synthesis of HDL,⁴² which effectively remove lipids from peripheral tissues (particularly sWAT and vWAT) to liver. Both improved lipolysis and lipid removal lead to reduction of mass and adipocyte size of vWAT. Lipids carried into the liver are then consumed by adiponectin-stimulated FFA oxidation without causing lipid accumulation in liver (Figure S27). Mass reduction of both sWAT and vWAT also improves systemic insulin sensitivity because their release of deleterious factors (e.g., FFA, inflammatory cytokines) is decreased. Taken together, through the crosstalks with other organs (e.g., liver) and tissues (e.g., visceral fat depots), ameliorating remodeling of sWAT improves whole-body energy metabolism.

CONCLUSIONS

All US-FDA approved medications for obesity indirectly act on the central nervous system to suppress appetite or on the gastrointestinal tract to inhibit fat absorption. Most of them have been withdrawn from the market because of serious side effects. Although laser lipolysis (actually ablation) and liposuction methods are performed in clinics to effectively remove targeted sWAT, they suffer from invasiveness, high cost, associated risks, induction of compensatory increase of vWAT,⁵⁰ and incapability of improving whole-body metabolism. In contrast, transdermal mPTT-PCT directly acts on the root of evil (sWAT depot) to trigger its ameliorating remodeling. In summary, this therapy can totally inhibit obesity development in high-fat-diet fed mice. It not only locally induces sWAT remodeling at the application site as evidenced by mass reduction, browning, lipolysis, apoptosis, and angiogenesis but also significantly improves systemic metabolism as evidenced by mass reduction of visceral fat, decrease of serum levels of cholesterol/triglyceride/insulin/glucose, and improved insulin sensitivity. Interestingly, vWAT reduction is more significant likely because it has a larger capacity for lipolysis than sWAT.⁵¹

Based on the mouse experiments, we envision that an obese patient at home could self-inject the therapeutics into belly fat at multiple sites using an insulin needle or an automated injection device equipped with hollow microneedle array once a week (Scheme 1). Subsequently, NIR irradiation for only 5 min at each application site using a hand-held laser source would be applied 1–3 times a day for several days. Significant outcome is expected after several week's treatment. This strategy may be paradigm-shifting because of its high effectiveness, convenience, and good patient compliance.

Recently, the Nie group has demonstrated an effective photodynamic therapy by irradiating mouse intra-abdominal fat to elicit ROS burst, thereby inducing apoptosis and lipolysis, after IV injection of the photodynamic agent and rosiglitazone, which has both browning and angiogenesis effects.⁵² But for human application of this method, a surgical procedure would be required to treat visceral fat. In comparison, our transdermal

strategy is more convenient. Such localized and targeted therapy not only minimizes side effects but also remotely leads to significant reduction of visceral fat and other improvements in systemic metabolism. Also noteworthy, it does not cause skin injury, pain, inflammatory response, fat accumulation in liver due to release of FFA and triglycerides, or toxicity in major organs. On the basis of the effective dosage of CuS-ND for mouse, the amount of copper needed for human therapy (according to the volume ratio between abdominal sWAT of an obese person and IgWAT of an obese mouse) is estimated to be 4–9 mg per day, which is lower than the safe threshold of copper intake (10 mg per day, about the amount in a slice of beef liver). In addition, as copper concentration in mouse serum was significantly less than the toxic level, the same is expected for human. Alternative to CuS-NDs, other inorganic degradable nanoparticles or organic NIR-absorbing dyes (e.g., indocyanine) may also be used as the mPTT agent. Here we repurposed an FDA-approved drug, mirabegron, as the browning and insulin-sensitizing agent. The dose needed in mPTT-PCT for human (~8 mg/day) is significantly lower than the FDA recommended dose (50 mg/day). The thorough documentation on its toxicity shall greatly lower the hurdle for its clinical use for obesity. Alternatively, other browning agents and metabolic activators (e.g., rosiglitazone) may also be used.

Skin is the readily accessible window for a wide range of theranostic purposes.⁵³ The herein demonstrated transdermal therapy could also be used for other medical problems. Further, we have revealed the multiple interconnected signaling pathways underlying our method that explains high effectiveness, synergy arising from the combined therapy, and systemic effects produced by localized treatment. The study provides key insights from systems point of view on adipobiology, crosstalks between metabolically active tissues, and developing effective strategies to combat obesity and other metabolic disorders.

METHODS

Synthesis, Functionalization, And Characterization of CuS Nanodots (CuS-NDs). A 50 mL solution with copper chloride dihydrate (CuCl₂·2H₂O, 1 mM) and sodium citrate (0.7 mM) was stirred for 30 min, followed by addition of 50 mL of sodium sulfide solution (Na₂S, 3 M). The mixture was then heated to 90 °C under stirring and kept for reaction for 15 min to produce dark green aqueous dispersion of CuS-NDs. The morphology and absorption spectra of Cu-NDs were analyzed by a transmission electronic microscope (JEM-2100PLUS, JEOL) and a spectrophotometer (UV-1800, Shimadzu), respectively. For some experiments, fluorescence dye Cy5 was conjugated with CuS-ND (Cy5-CuS). Briefly, 30.24 μ M (1-ethyl-3-(3-(dimethylamino)propyl)carbodiimide hydrochloride) (EDC) and 30.24 μ M (N-hydroxysulfosuccinimide) (NHS) were added into 9 mL of CuS-ND solution and stirred for 30 min to activate carboxylate groups on CuS-ND surface. Cy5-amine (25 mg/mL, 9 μ L) was then added to the solution with stirring for 12 h, followed by dialysis (5 kDa) for 24 h to remove free Cy5 molecules. For some experiments, adipose-homing peptide (CKGGRAKDC) was grafted onto CuS-NDs using the same chemistry. CuS-gel was fabricated by mixing CuS-NDs with F127 (25%) and HA (1%) under overnight stirring at 4 °C.

Primary Cells and Animals. Primary human white preadipocytes isolated from adult subcutaneous WAT were purchased from Zen-Bio, Inc. Cells were grown in DMEM/F-12 (1:1, v/v) medium containing 10% fetal bovine serum (FBS) under a 5% CO₂ atmosphere at 37 °C. Mice (C57BL/6J, 7- to 8-week-old male, average body weight of 25.1 g) were purchased from Animal Research Facility of Nanyang Technological University, and housed in the holding room with light/dark cycle (12 h/12 h) and temperature control at 23.5 °C. Food and water are always available. All of the animal experiments were performed in accordance with ethical approval by the Institutional

Animal Care and Use Committee of Nanyang Technological University (NTU-IACUC, A18029).

In Vitro Experiments on Human Subcutaneous White Adipocytes. Adipocytes were incubated in DMEM/F-12 medium, without any treatment (control) or treated with CuS-gel (20 μ L containing 0.5 mg/mL CuS-NDs) or CuS-NDs without gel encapsulation (same amount of CuS-NDs as in CuS-gel) for 12 h. The adipocytes were then irradiated with an NIR laser (Shanghai Connet Fiber Optics; 1064 nm, 0.4 W/cm²) for 5 min. After 12 h, apoptotic cells were identified by DeadEnd Fluorometric TUNEL kit (Promega). Released free fatty acid (FFA) was analyzed using a colorimetric quantification kit (Sigma-Aldrich). Intracellular lipid droplets were stained with Oil Red O (Sigma-Aldrich) and imaged using an inverted microscope (Olympus IX71). Twenty-four hours after NIR irradiation, adipocytes were stained with specific primary antibodies (UCP1, HSL, ATGL; 1:50 dilution; Thermo Fisher Scientific) and further incubated with fluorescence dye conjugated secondary antibody (1:1000–2000, Thermo Fisher Scientific). Immunofluorescence staining was visualized by a confocal laser scanning microscope (CLSM) (LSM800, Carl Zeiss). After being incubated with CuS-gel, adipocytes were then incubated with a Ca²⁺ indicator (Fluo-8 AM, 5 mM) for 1 h in darkness. Subsequently, they were washed with the medium followed by adding CaCl₂ solution (2 mM). A 1064 nm NIR laser (0.4 W/cm²) was irradiated on the adipocytes, and fluorescence images were recorded in real-time at 37 °C using CLSM (Ex: 488 nm, Em: 525 nm).

In Vivo Fluorescence Imaging. To reveal the biodistribution of Cy5-CuS (25 μ g) delivered by different methods, mice were subcutaneously injected with CuS-gel at the inguinal region, intravenously injected with Cy5-CuS, or applied with a microneedle (MN) patch loaded with Cy5-CuS at the inguinal region. After 1 or 24 h, fat tissues and major organs (IgWAT, interscapular BAT, EpiWAT, kidney, heart, lung, liver, spleen, and skin on application sites) were visualized by an *in vivo* imaging system (IVIS Spectrum, PerkinElmer) using a filter set (excitation at 640 nm, emission at 680 nm). To investigate the release profiles, mice were subcutaneously injected with F127/HA gel or PBS containing Cy5 or Cy5-CuS at the inguinal region and imaged under IVIS at different days.

In Vivo Biocompatibility and Safety Evaluation. Mice were treated without (control) or with subcutaneous injection of CuS-gel (50 μ L loaded with 25 μ g CuS-NDs) once a week at both sides of inguinal regions, or subcutaneous injection of CuS-gel, followed by NIR irradiation (1064 nm, 0.4 W/cm², 5 min for 3 consecutive days) and 4 days of rest. Such one-week treatment course was repeated in the second week. After treatment, the harvested organs were fixed in 4% paraformaldehyde for 24 h, incubated in 30% sucrose for 2 days, and then frozen and embedded in FSC22 frozen section medium (Leica Biosystems). Slices with \sim 10 μ m thickness were cut using a cryostat (CM1950 cryostat, Leica Microsystems) and then stained with hematoxylin and eosin (H&E) solution (Sigma-Aldrich). Images were obtained using a digital microscope (Leica DVM6). Moreover, serum levels of aspartate transaminase (AST), alanine transaminase (ALT), blood urea nitrogen (BUN), and creatinine (CRE) as well as blood hemoglobin (HGB) were measured by colorimetric quantification kits (Sigma-Aldrich). Red blood cells (RBC) and platelets (PLT) were manually counted under an inverted microscope. Blood hematocrit (HPCT) was calculated by taking the ratio of the volume of packed erythrocytes to the total volume of the blood sample in the capillary tube after centrifugation (4000 rpm, 10 min). Mean corpuscular volume (MCV), mean corpuscular hemoglobin (MCH), and mean corpuscular hemoglobin concentration (MCHC) were calculated according to the standard equations. After CuS-gel injection, mice were transferred into metabolic cages. The collected urine (0.2 mL) or serum (0.05 mL) was mixed with nitric acid (0.6 or 0.75 mL), which was then added into deionized water (10.2 mL) for determining copper concentration by inductively coupled plasma mass spectrometer (ICP-MS, PerkinElmer).

In Vivo Treatment. Mice were fed with a high-fat diet (58Y1, 60% kcal from fat, Testdiet) for 3 weeks. Then the obese mice with an average body weight of 30.8 g were randomly divided into groups for

different treatments. Mice were treated without (control) or with NIR laser irradiation alone (1064 nm, 0.4 W/cm², 5 min; 3 consecutive days) or subcutaneous injection of CuS-gel (CuS-L, 1.5 mg/kg of CuS-NDs, or CuS-H, 3 mg/kg of CuS-NDs; once a week) followed by NIR laser irradiation, or subcutaneous injection of capsaicin gel (Cap, 3 mg/kg; once a week), or subcutaneous injection of mirabegron gel (Mir, 0.75 mg/kg; once a week), or subcutaneous injection of mirabegron-encapsulated CuS-gel (CuS-NDs, 1.5 mg/kg; Mir, 0.75 mg/kg; once a week) followed by NIR laser irradiation. A thermal image was recorded on the shaved skin using an infrared camera (T420, FLIR). All treatments were performed under anesthesia (\sim 10 min). To access possible pain, mouse behaviors were monitored using Grimace scoring based on orbital tightening, nose bulge, check bulge, and ear position. For the glucose tolerance test at day 12 of treatment, fasted mice (overnight, 12 h) were intraperitoneally injected with glucose solution (1 g/kg in PBS) before measuring blood glucose concentrations in tail veins at different time points with a glucometer (Accu-Chek Performa, Roche). At day 14, body surface temperature was recorded on the shaved skin under fully awake condition using an infrared camera (T420, FLIR). Blood was collected for the assessment of serological parameters using a mouse enzyme-linked immunosorbent assay (ELISA) kit (Abcam or Thermo Fisher Scientific) or colorimetric quantification kits (Sigma-Aldrich). Mice were then euthanized, and fat tissues (IgWAT, EpiWAT, interscapular BAT) and major organs (liver, kidneys, spleen, lung, heart) were excised, weighed, and fixed for H&E staining and immunohistological analyses. IgWAT slices were evaluated by DeadEnd Fluorometric TUNEL kit (Promega), or immunostained with anti-UCP1 antibody (1:50 dilution, Thermo Fisher Scientific) or anti-CD31 antibody (1:50 dilution, Santa Cruz Biotechnology) for visualization by CLSM. Some portions of IgWATs were homogenized in radioimmunoprecipitation assay buffer (containing protease inhibitor cocktail, Roche) for immunoblot analyses.

Statistical Analyses. Quantitative results are represented as the mean \pm standard deviation (s.d.), indicated by error bars in all graphs. Statistical analyses were conducted using GraphPad Prism 7. Unpaired two-tailed Student's *t* test or one-way analysis of variance (ANOVA) was used for data analyses. A *P* value of less than 0.05 was considered statistically significant (**P* < 0.05, ***P* < 0.01, ****P* < 0.001).

ASSOCIATED CONTENT

Supporting Information

The Supporting Information is available free of charge at <https://pubs.acs.org/doi/10.1021/acsnano.1c06410>.

Additional materials and methods, *in vitro* characterization of CuS-ND and CuS-gel, schematic illustration of CuS-ND synthesis and gel formation, *in vitro* photothermal effects of CuS-gel, *in vitro* assessment for mPTT effects of CuS-ND on human subcutaneous white adipocytes, quantification of immunostained and Western blot images, quantification of fluorescence intensity of IVIS images, histological analysis of major organs, biosafety and skin safety assessment, *ex vivo* photothermal effects of mice skin and inguinal white adipose tissue, additional quantification of body surface temperature, body weight, food intake, urine and feces, sizes of adipocytes, and serum markers, analysis of lipases expression, and *in vivo* assessment of fat accumulation in liver (PDF)

AUTHOR INFORMATION

Corresponding Author

Peng Chen – School of Chemical and Biomedical Engineering, Nanyang Technological University, 637457, Singapore; Lee Kong Chian School of Medicine, Nanyang Technological University, 636921, Singapore; Skin Research Institute of

Singapore, 308232, Singapore; orcid.org/0000-0003-3730-1846; Email: chenpeng@ntu.edu.sg

Authors

Ping Zan – School of Chemical and Biomedical Engineering, Nanyang Technological University, 637457, Singapore

Aung Than – School of Chemical and Biomedical Engineering, Nanyang Technological University, 637457, Singapore; orcid.org/0000-0003-1558-7310

Weiqing Zhang – School of Chemical and Biomedical Engineering, Nanyang Technological University, 637457, Singapore; Affiliated Tumor Hospital, Guangxi Medical University, Nanning 530021, P.R. China; orcid.org/0000-0002-1324-2944

Helen Xinyi Cai – University of Cambridge, The Old Schools, Cambridge CB2 1TN, United Kingdom

Wenting Zhao – School of Chemical and Biomedical Engineering, Nanyang Technological University, 637457, Singapore; orcid.org/0000-0002-6143-5185

Complete contact information is available at: <https://pubs.acs.org/10.1021/acsnano.1c06410>

Author Contributions

[‡]P.Z. and A.T. contributed equally. P. Z. and A. T. conceived, designed, and carried out the experiments. W. Zhang, H. C. and W. Zhao contribute to materials synthesis/characterizations and data interpretation. P. C. supervised the study and revised the manuscript. All authors have given approval to the final version of the manuscript.

Funding

This work was financially supported by the Singapore Ministry of Education under its Academic Research Fund (AcRF) Tier-1 grants (RG110/20 and RT02/20) and AcRF Tier-2 grant (MOE2019-T2-2-004).

Notes

The authors declare no competing financial interest.

ACKNOWLEDGMENTS

We acknowledge support from Innovative Centre for Flexible Devices at Nanyang Technological University. We also acknowledge Servier Medical Art (<https://smart.servier.com>) for providing cartoons of mice and some components.

REFERENCES

- (1) Chouchani, E. T.; Kajimura, S. Metabolic Adaptation and Maladaptation in Adipose Tissue. *Nat. Metab.* **2019**, *1*, 189–200.
- (2) Kopelman, P. G. Obesity as a Medical Problem. *Nature* **2000**, *404*, 635–643.
- (3) Olson, O. C.; Quail, D. F.; Joyce, J. A. Obesity and the Tumor Microenvironment. *Science* **2017**, *358*, 1130–1131.
- (4) Heymsfield, S. B.; Wadden, T. A. Mechanisms, Pathophysiology, and Management of Obesity. *N. Engl. J. Med.* **2017**, *376*, 254–266.
- (5) Ouchi, N.; Parker, J. L.; Lugus, J. J.; Walsh, K. Adipokines in Inflammation and Metabolic Disease. *Nat. Rev. Immunol.* **2011**, *11*, 85–97.
- (6) Srivastava, G.; Apovian, C. M. Current Pharmacotherapy for Obesity. *Nat. Rev. Endocrinol.* **2018**, *14*, 12–24.
- (7) Al Dujaili, Z.; Karcher, C.; Henry, M.; Sadick, N. Fat Reduction: Complications and Management. *J. Am. Acad. Dermatol.* **2018**, *79*, 197–205.
- (8) Dietrich, M. O.; Horvath, T. L. Limitations in Anti-Obesity Drug Development: The Critical Role of Hunger-Promoting Neurons. *Nat. Rev. Drug Discovery* **2012**, *11*, 675–691.
- (9) Nguyen, N. T.; Varela, J. E. Bariatric Surgery for Obesity and Metabolic Disorders: State of the Art. *Nat. Rev. Gastroenterol. Hepatol.* **2017**, *14*, 160.
- (10) Betz, M. J.; Enerbäck, S. Targeting Thermogenesis in Brown Fat and Muscle to Treat Obesity and Metabolic Disease. *Nat. Rev. Endocrinol.* **2018**, *14*, 77.
- (11) Bartelt, A.; Heeren, J. Adipose Tissue Browning and Metabolic Health. *Nat. Rev. Endocrinol.* **2014**, *10*, 24.
- (12) Than, A.; Duong, P. K.; Zan, P.; Liu, J.; Leow, M. K. S.; Chen, P. Lancing Drug Reservoirs into Subcutaneous Fat to Combat Obesity and Associated Metabolic Diseases. *Small* **2020**, *16*, 2002872.
- (13) Xue, Y.; Xu, X.; Zhang, X.-Q.; Farokhzad, O. C.; Langer, R. Preventing Diet-Induced Obesity in Mice by Adipose Tissue Transformation and Angiogenesis Using Targeted Nanoparticles. *Proc. Natl. Acad. Sci. U. S. A.* **2016**, *113*, 5552–5557.
- (14) Than, A.; Xu, S.; Li, R.; Leow, M.-S.; Sun, L.; Chen, P. Angiotensin Type 2 Receptor Activation Promotes Browning of White Adipose Tissue and Brown Adipogenesis. *Signal Transduct. Target Ther.* **2017**, *2*, 1–12.
- (15) Sun, K.; Kusminski, C. M.; Scherer, P. E. Adipose Tissue Remodeling and Obesity. *J. Clin. Investig.* **2011**, *121*, 2094–2101.
- (16) Luo, Z.; Ma, L.; Zhao, Z.; He, H.; Yang, D.; Feng, X.; Ma, S.; Chen, X.; Zhu, T.; Cao, T. TRPV1 Activation Improves Exercise Endurance and Energy Metabolism through PGC-1 α Upregulation in Mice. *Cell Res.* **2012**, *22*, 551–564.
- (17) Ahern, G. P. Transient Receptor Potential Channels and Energy Homeostasis. *Trends Endocrinol. Metab.* **2013**, *24*, 554–560.
- (18) Shamsi, F.; Piper, M.; Ho, L.-L.; Huang, T. L.; Gupta, A.; Streets, A.; Lynes, M. D.; Tseng, Y.-H. Vascular Smooth Muscle-Derived Trpv1⁺ Progenitors Are a Source of Cold-Induced Thermogenic Adipocytes. *Nat. Metab.* **2021**, *3*, 485–495.
- (19) Baskaran, P.; Krishnan, V.; Ren, J.; Thyagarajan, B. Capsaicin Induces Browning of White Adipose Tissue and Counters Obesity by Activating TRPV1 Channel-Dependent Mechanisms. *Br. J. Pharmacol.* **2016**, *173*, 2369–2389.
- (20) Suri, A.; Szallasi, A. The Emerging Role of TRPV1 in Diabetes and Obesity. *Trends Pharmacol. Sci.* **2008**, *29*, 29–36.
- (21) Holmes, D. 'Hot' and Cold Therapy Reduces Obesity. *Nat. Rev. Endocrinol.* **2016**, *12*, 248–248.
- (22) Zsiborás, C.; Mátics, R.; Hegyi, P.; Balaskó, M.; Pétervári, E.; Szabó, I.; Sarlós, P.; Mikó, A.; Tenk, J.; Rostás, I. Capsaicin and Capsiate Could Be Appropriate Agents for Treatment of Obesity: A Meta-Analysis of Human Studies. *Crit. Rev. Food Sci. Nutr.* **2018**, *58*, 1419–1427.
- (23) Bode, A. M.; Dong, Z. The Two Faces of Capsaicin. *Cancer Res.* **2011**, *71*, 2809–2814.
- (24) Caterina, M. J.; Schumacher, M. A.; Tominaga, M.; Rosen, T. A.; Levine, J. D.; Julius, D. The Capsaicin Receptor: A Heat-Activated Ion Channel in the Pain Pathway. *Nature* **1997**, *389*, 816–824.
- (25) Gao, W.; Sun, Y.; Cai, M.; Zhao, Y.; Cao, W.; Liu, Z.; Cui, G.; Tang, B. Copper Sulfide Nanoparticles as a Photothermal Switch for TRPV1 Signaling to Attenuate Atherosclerosis. *Nat. Commun.* **2018**, *9*, 1–10.
- (26) Yun, S. H.; Kwok, S. J. Light in Diagnosis, Therapy and Surgery. *Nat. Biomed. Eng.* **2017**, *1*, 1–16.
- (27) Xu, C.; Pu, K. Second Near-Infrared Photothermal Materials for Combinational Nanotheranostics. *Chem. Soc. Rev.* **2021**, *143*, 11277.
- (28) Dong, C.; Feng, W.; Xu, W.; Yu, L.; Xiang, H.; Chen, Y.; Zhou, J. The Coppery Age: Copper (Cu)-Involved Nanotheranostics. *Adv. Sci.* **2020**, *7*, 2001549.
- (29) Li, Y.; Lu, W.; Huang, Q.; Li, C.; Chen, W. Copper Sulfide Nanoparticles for Photothermal Ablation of Tumor Cells. *Nanomedicine* **2010**, *5*, 1161–1171.
- (30) Zhou, M.; Li, J.; Liang, S.; Sood, A. K.; Liang, D.; Li, C. CuS Nanodots with Ultrahigh Efficient Renal Clearance for Positron Emission Tomography Imaging and Image-Guided Photothermal Therapy. *ACS Nano* **2015**, *9*, 7085–7096.
- (31) Jung, Y.-s.; Park, W.; Park, H.; Lee, D.-K.; Na, K. Thermo-Sensitive Injectable Hydrogel Based on the Physical Mixing of

- Hyaluronic Acid and Pluronic F-127 for Sustained NSAID Delivery. *Carbohydr. Polym.* **2017**, *156*, 403–408.
- (32) Kolonin, M. G.; Saha, P. K.; Chan, L.; Pasqualini, R.; Arap, W. Reversal of Obesity by Targeted Ablation of Adipose Tissue. *Nat. Med.* **2004**, *10*, 625–632.
- (33) Ma, L.; Liu, T.-W.; Wallig, M. A.; Dobrucki, I. T.; Dobrucki, L. W.; Nelson, E. R.; Swanson, K. S.; Smith, A. M. Efficient Targeting of Adipose Tissue Macrophages in Obesity with Polysaccharide Nanocarriers. *ACS Nano* **2016**, *10*, 6952–6962.
- (34) Than, A.; Liu, C.; Chang, H.; Duong, P. K.; Cheung, C. M. G.; Xu, C.; Wang, X.; Chen, P. Self-Implantable Double-Layered Micro-Drug-Reservoirs for Efficient and Controlled Ocular Drug Delivery. *Nat. Commun.* **2018**, *9*, 1–12.
- (35) Zan, P.; Than, A.; Duong, P. K.; Song, J.; Xu, C.; Chen, P. Antimicrobial Microneedle Patch for Treating Deep Cutaneous Fungal Infection. *Adv. Ther.* **2019**, *2*, 1900064.
- (36) Than, A.; Liang, K.; Xu, S.; Sun, L.; Duan, H.; Xi, F.; Xu, C.; Chen, P. Transdermal Delivery of Anti-Obesity Compounds to Subcutaneous Adipose Tissue with Polymeric Microneedle Patches. *Small Methods* **2017**, *1*, 1700269.
- (37) Zhang, Y.; Liu, Q.; Yu, J.; Yu, S.; Wang, J.; Qiang, L.; Gu, Z. Locally Induced Adipose Tissue Browning by Microneedle Patch for Obesity Treatment. *ACS Nano* **2017**, *11*, 9223–9230.
- (38) Bao, C.; Li, Z.; Liang, S.; Hu, Y.; Wang, X.; Fang, B.; Wang, P.; Chen, S.; Li, Y. Microneedle Patch Delivery of Capsaicin-Containing α -Lactalbumin Nanomicelles to Adipocytes Achieves Potent Anti-Obesity Effects. *Adv. Funct. Mater.* **2021**, *31*, 2011130.
- (39) Shi, S.; Wen, X.; Li, T.; Wen, X.; Cao, Q.; Liu, X.; Liu, Y.; Pagel, M. D.; Li, C. Thermosensitive Biodegradable Copper Sulfide Nanoparticles for Real-Time Multispectral Optoacoustic Tomography. *ACS Appl. Bio Mater.* **2019**, *2*, 3203–3211.
- (40) Straub, L. G.; Scherer, P. E. Metabolic Messengers: Adiponectin. *Nat. Metab.* **2019**, *1*, 334–339.
- (41) Maeda, N.; Takahashi, M.; Funahashi, T.; Kihara, S.; Nishizawa, H.; Kishida, K.; Nagaretani, H.; Matsuda, M.; Komuro, R.; Ouchi, N. PPAR γ Ligands Increase Expression and Plasma Concentrations of Adiponectin, an Adipose-Derived Protein. *Diabetes* **2001**, *50*, 2094–2099.
- (42) Christou, G.; Kiortsis, D. Adiponectin and Lipoprotein Metabolism. *Obes. Rev.* **2013**, *14*, 939–949.
- (43) Dehvari, N.; da Silva Junior, E. D.; Bengtsson, T.; Hutchinson, D. S. Mirabegron: Potential Off Target Effects and Uses beyond the Bladder. *Br. J. Pharmacol.* **2018**, *175*, 4072–4082.
- (44) Finlin, B. S.; Memetimin, H.; Zhu, B.; Confides, A. L.; Vekaria, H. J.; El Khouli, R. H.; Johnson, Z. R.; Westgate, P. M.; Chen, J.; Morris, A. J. The β 3-Adrenergic Receptor Agonist Mirabegron Improves Glucose Homeostasis in Obese Humans. *J. Clin. Investig.* **2020**, *130*, 2319.
- (45) Okeke, K.; Angers, S.; Bouvier, M.; Michel, M. C. Agonist-Induced Desensitisation of β 3-Adrenoceptors: Where, When, and How? *Br. J. Pharmacol.* **2019**, *176*, 2539–2558.
- (46) Mahamid, J.; Tegunov, D.; Maiser, A.; Arnold, J.; Leonhardt, H.; Plitzko, J. M.; Baumeister, W. Liquid-Crystalline Phase Transitions in Lipid Droplets Are Related to Cellular States and Specific Organelle Association. *Proc. Natl. Acad. Sci. U. S. A.* **2019**, *116*, 16866–16871.
- (47) Gérard, C.; Bordeleau, L.-J.; Barralet, J.; Doillon, C. J. The Stimulation of Angiogenesis and Collagen Deposition by Copper. *Biomaterials* **2010**, *31*, 824–831.
- (48) Ouchi, N.; Kobayashi, H.; Kihara, S.; Kumada, M.; Sato, K.; Inoue, T.; Funahashi, T.; Walsh, K. Adiponectin Stimulates Angiogenesis by Promoting Cross-Talk between Amp-Activated Protein Kinase and Akt Signaling in Endothelial Cells. *J. Biol. Chem.* **2004**, *279*, 1304–1309.
- (49) Cao, Y. Angiogenesis and Vascular Functions in Modulation of Obesity, Adipose Metabolism, and Insulin Sensitivity. *Cell Metab.* **2013**, *18*, 478–489.
- (50) Benatti, F.; Solis, M.; Artioli, G.; Montag, E.; Painelli, V.; Saito, F.; Baptista, L.; Costa, L. A.; Neves, R.; Seelaender, M. Liposuction Induces a Compensatory Increase of Visceral Fat Which Is Effectively

Counteracted by Physical Activity: A Randomized Trial. *J. Clin. Endocrinol. Metab.* **2012**, *97*, 2388–2395.

(51) Ibrahim, M. M. Subcutaneous and Visceral Adipose Tissue: Structural and Functional Differences. *Obes. Rev.* **2010**, *11*, 11–18.

(52) Chen, R.; Huang, S.; Lin, T.; Ma, H.; Shan, W.; Duan, F.; Lv, J.; Zhang, J.; Ren, L.; Nie, L. Photoacoustic Molecular Imaging-Escorted Adipose Photodynamic–Browning Synergy for Fighting Obesity with Virus-Like Complexes. *Nat. Nanotechnol.* **2021**, *16*, 455–465.

(53) Than, A.; Zan, P.; Chen, P. Transdermal Theranostics. *View* **2020**, *1*, e21.



ACS IN FOCUS

Cellular Agriculture
Lab-Grown
Dilek Erilci-C
Dorothee E

Machine Learning in Chemistry
Jon Paul Janet &
Heather J. Kulik

bacterials
Lidia Cheng Jaramillo
William M. Wuest

ACS In Focus ebooks are digital publications that help readers of all levels accelerate their fundamental understanding of emerging topics and techniques from across the sciences.

pubs.acs.org/series/infocus

ACS Publications
Most Trusted. Most Cited. Most Read.

QR code